Acta Oceanol. Sin., 2016, Vol. 35, No. 9, P. 80–85
DOI: 10.1007/s13131-016-0936-4
http://www.hyxb.org.cn
E-mail: hyxbe@263.net

Satellite SAR observation of the sea surface wind field caused by rain cells

YE Xiaomin[1, 2, 3], LIN Mingsen[2, 3]*, YUAN Xinzhe[2, 3], DING Jing[2, 3], XIE Xuetong[4], ZHANG Yi[2, 3]
XU Ying[1, 2, 3]

[1] College of Information Science and Engineering, Ocean University of China, Qingdao 266100, China

[2] National Satellite Ocean Application Service, State Oceanic Administration, Beijing 100081, China

[3] Key Laboratory of Space Ocean Remote Sensing and Application, State Oceanic Administration, Beijing 100081, China

[4] School of Geographical Sciences, Guangzhou University, Guangzhou 510006, China

Received 14 September 2015; accepted 9 November 2015

Abstract

Rain cells or convective rain, the dominant form of rain in the tropics and subtropics, can be easy detected by satellite Synthetic Aperture Radar (SAR) images with high horizontal resolution. The footprints of rain cells on SAR images are caused by the scattering and attenuation of the rain drops, as well as the downward airflow. In this study, we extract sea surface wind field and its structure caused by rain cells by using a RADARSAT-2 SAR image with a spatial resolution of 100 m for case study. We extract the sea surface wind speeds from SAR image by using CMOD4 geophysical model function with outside wind directions of NCEP final operational global analysis data, Advance Scatterometer (ASCAT) onboard European MetOp-A satellite and microwave scatterometer onboard Chinese HY-2 satellite, respectively. The root-mean-square errors (RMSE) of these SAR wind speeds, validated against NCEP, ASCAT and HY-2, are 1.48 m/s, 1.64 m/s and 2.14 m/s, respectively. Circular signature patterns with brighter on one side and darker on the opposite side on SAR image are interpreted as the sea surface wind speed (or sea surface roughness) variety caused by downdraft associated with rain cells. The wind speeds taken from the transect profile which superposes to the wind ambient vectors and goes through the center of the circular footprint of rain cell can be fitted as a cosine or sine curve in high linear correlation with the values of no less than 0.80. The background wind speed, the wind speed caused by rain cell and the diameter of footprint of the rain cell with kilometers or tens of kilometers can be acquired by fitting curve. Eight cases interpreted and analyzed in this study all show the same conclusion.

Key words: rain cells, Synthetic Aperture Radar (SAR), sea surface wind field, downdraft

Citation: Ye Xiaomin, Lin Mingsen, Yuan Xinzhe, Ding Jing, Xie Xuetong, Zhang Yi, Xu Ying. 2016. Satellite SAR observation of the sea surface wind field caused by rain cells. Acta Oceanologica Sinica, 35(9): 80–85, doi: 10.1007/s13131-016-0936-4

1 Introduction

Rainfall is one of the most important atmospheric phenomena that can strongly impact the local weather. Rain can occur as stratiform rain or convective rain (rain cells). Stratiform rain is the dominant from of rain in the high latitudes, while convective rain is the dominant form of rain in the tropics and subtropics (Houze Jr, 1997). Rain cells can be easy detected by satellite Synthetic Aperture Radar (SAR) images of the ocean surface with high horizontal resolution ($\leqslant$100 m) (Alpers and Melsheimer, 2004). The footprints of rain cells are usually observed and studied by SAR and simultaneous ground-based weather radar data (e.g., Friedman and Li, 2000; Melsheimer et al., 2001; Lin et al., 2001; Alpers et al., 2007; Gan et al., 2007; Chan et al., 2010; Xu et al., 2015). The footprints of rain cells on SAR images are caused by the scattering and attenuation of the rain drops, as well as the local downward airflow and the background sea surface wind (Alpers and Melsheimer, 2004; Contreras and Plant, 2006; Xu et al., 2015). CMOD4 is a geophysical model function (GMF) of sea surface wind retrieval for microwave scatterometer remote sensing data (Stofflen and Anderson, 1997). It is also widely used in high spatial resolution coastal wind retrieval from the SAR image (e.g., Thompson et al., 2001; Yang et al., 2001; Xu et al., 2008; Lin et al., 2008; Morena et al., 2004; Zhang et al., 2014). C-band radar signatures of rain cells with rain rates below 50 mm/h are mainly caused by a modification of sea surface roughness induced the raindrops impinging on the sea surface and local wind field associated with rain cells (Melsheimer et al., 2001).

In this study, we extract sea surface wind speeds by using CMOD4 GMF from A RASASAT-2 SAR image firstly, then we validate them against referenced sea surface wind speed to make sure the wind retrieval method in this study are reliable. A last, we extract the local wind speeds of the footprint signature patterns caused by rain cells on SAR image for case study and analyse their feature.

Foundation item: The Joint Foundation of National Natural Science Foundation of China and the Marine Science Center of Shandong Province under contract No. U1406404; the National Natural Science Foundation of China under contract Nos 41506206, 41306186 and 41476152; the Global Change and Air-Sea Interaction Project of China under contract No. GASI-03-03-01-01; the Open funds of State Key Laboratory of Satellite Ocean Environment Dynamics under contract No. SOED1411.
*Corresponding author, E-mail: mslin@mail.nsoas.org.cn

2 Data and wind retrieval method

2.1 *Satellite SAR image data*

The satellite SAR images used in this study were taken by Canadian RADARSAR-2 satellite, an earth observation satellite launched on December 14, 2007. RADARSAR -2 carries a single sensor C-band (5.405 GHz) SAR with HH, HV, VV and VH polarization modes and multiple scanning modes (Morena et al., 2008). The image shown in Fig. 1 was acquired by ScanSAR Wide Beam mode and VV polarization with a nominal swath width of 500 km and a spatial resolution of 100 m. The imaging time was 22:20 UTC on May 24, 2012.

As shown in the right sub-image in Fig. 1, a typical SAR signature of airflow footprint pattern caused by the downdraft of rain cell is obvious, i.e., the circular or elliptical pattern is usually less bright in the center and brighter than the surrounding area on one side and darker on the opposite side (Alpers and Melsheimer, 2004).

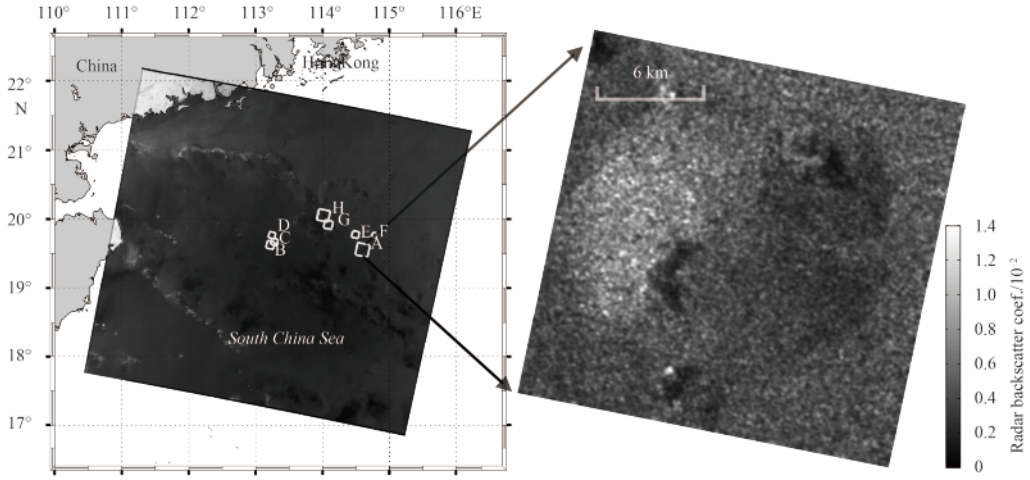

Fig. 1. RADARSAR-2 SAR image (C-band, VV polarization) acquired on May 24, 2012, 22:20 UTC covers South China Sea. The eight white square frames with No. A–H on the left are the signature patterns of rain cells. The sub-image on the right is the normalized radar cross section (NRCS) image of Pattern A.

2.2 *Sea surface wind field data*

To get the initialization of wind directions for wind retrieval model and validate the extracted sea surface wind speeds from SAR image, we use collocated NCEP, ASCAT and HY-2 microwave scatterometer (HY-2 SCAT) sea surface wind field data in this study.

The National Centers for Environmental Prediction (NCEP) final operational global analysis data (FNLs) are on 1-degree by 1-degree grids prepared operationally every six hours. This product is from the Global Data Assimilation System (GDAS), which continuously collects observational data from the Global Telecommunications System (GTS), and other sources, for many analyses. These NCEP reanalysis data are made with the same model which NCEP uses in the Global Forecast System (GFS), but they are prepared about an hour or so after the GFS is initialized. The data are delayed so that more observational data can be used. The GFS is run earlier in support of time critical forecast needs, and uses the FNL from the previous 6 hour cycle as part of its initialization. Sea surface wind speeds and directions can be extracted from these NCEP data. More description and the data can be found from http://rda.ucar.edu/.

Advanced Scatterometer (ASCAT) is a C-band (5.255 GHz) scatterometer carried on EUMETSAT MetOp-A and MetOp-B satellite. MetOp-A satellite was launched on October 19, 2006. It became fully operational in mid-May 2007 and continues to operate today. MetOp-B was launched on September 17, 2012. Both ASCATs onboard MetOp-A and MetOp-B are identical instruments. The main objective of ASCAT is measurement of wind speed and direction over global oceans. The operational wind speed and direction products with a resolution of 25 km and a swath of 500 km can be downloaded from https://podaac.jpl.nasa.gov/.

HY-2 microwave scatterometer (HY-2 SCAT) is a main payload carried by Chinese Haiyang-2 (HY-2) satellite, which is the first Chinese marine dynamic environment satellite, was launched at 22:57 UTC, on August 15, 2011. The payloads of HY-2 satellite include a dual-frequency radar altimeter operating at 13.58 GHz (Ku band) and 5.25 GHz (C band), DORIS, a microwave scatterometer, a scanning microwave radiometer and a calibration microwave radiometer. The objective of HY-2 is monitoring the dynamic ocean environment by using microwave sensors onboard. It is used to detect global sea surface wind field, sea surface height, significant wave height and sea surface temperature in all-weather. National Satellite Ocean Application Service (NSOAS), States Oceanic Administration (SOA) of China offers the HY-2 satellite data to public for free. The HY-2 SCAT, operating at Ku-band (13.256 GHz), has been working effective to provide operational sea surface wind speed and direction data for more than three years (October 1, 2011 to present). The level-2B HY-2 SCAT sea surface wind field data with a resolution of 25 km and a swath of more than 1 700 km (VV polarization) or 1 350 km (HH polarization) used in this study are offered by NSOAS (http://www.nsoas.org.cn/NSOAS_En/index.html) (Jiang et al., 2012; Ye et al., 2015).

2.3 *Wind retrieval method*

We extract the sea surface wind speed from the normalized radar cross section (NRCS) of SAR image. The wind retrieval method for SAR used in this study is CMOD4, a C-band GMF relating incident angle, wind speed and direction to NRCS (Stofflen and Anderson, 1997). The relationship form of the CMOD4 wind retrieval model function can be expressed as following:

$$\sigma_0{}^{vv} = f\,(V, \Phi, \theta)\,, \tag{1}$$

where V is the sea surface wind speed (unit: m/s), Φ is the relative direction (angle between the radar look direction and the real wind direction) in degree and θ is the radar wave incidence angle in degree. $\sigma_0{}^{vv}$ is the NRCS value in VV polarization, f is a nonlinear function and its expression can be found in Stofflen and Anderson (1997). Wind speed retrieval from HH polarized SAR can be achieved by the model function listed in Eq. (1) and the polarization ratio (Lin et al., 2008).

There are many other GMFs can be used for sea surface wind retrieval from SAR, such as CMOD-IFR2 and CMOD5 (Quilfen et al., 1998; Hersbach et al., 2007). Xu et al. (2008) evaluated the three C-band wind speed retrieval models (i.e., CMOD4, CMOD-IFR2 and CMOD5) by using ENVISAT ASAR VV-polarized data. Their results indicated that CMOD4 gave the best performance for sea surface wind speed retrievals in the coastal waters near Hong Kong (the same area as our study, as shown in Fig. 1 in this study and Fig. 1 in Xu et al. (2008)) at wind speed lower than 15 m/s (the same situation as ours, as shown in Fig. 2). For these reasons, CMOD4 is selected as a GMF in this study.

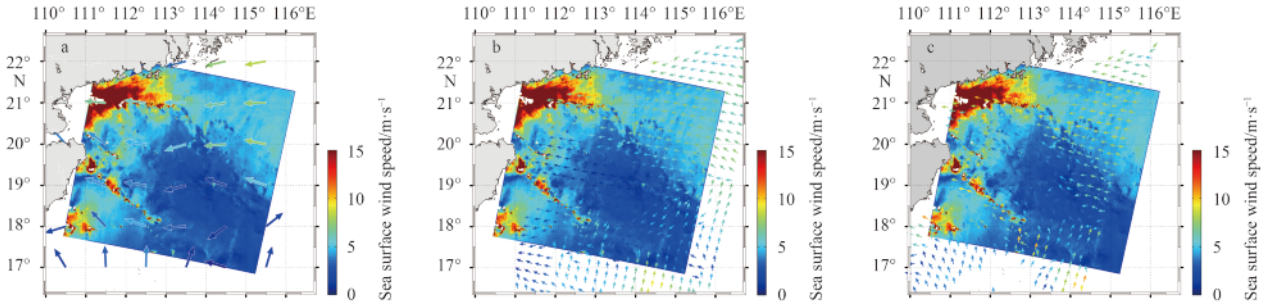

Fig. 2. Sea surface wind speed retrieval results from SAR image shown in Fig. 1. The color-coded arrows represent the outside winds vectors used for the SAR wind speed retrieval. a. NCEP on May 25, 2012 at 00:00 UTC, b. ASCAT on May 25, 2012 at 01:43 UTC and c. HY-2 SCAT on May 24, 19:21 UTC.

At a given wind speed and direction from radar geometry, the NRCS can be empirically predicted, but the inverse is not true, i.e., a given NRCS does not correspond to a unique wind speed and direction (Alpers and Melsheimer, 2004). With wind directions from either the wind directions features on SAR image itself (e.g., wind shadowing or wind streaks) or from outside wind sources (e.g., *in situ* data, remote sensing measurements or atmospheric model output) and the GMF, the wind speed can be derived from the NRCS of SAR image (Lin et al., 2008). In this study, we use the wind directions of NCEP final operational global analysis data, advance scatterometer (ASCAT) onboard European MetOp-A satellite and microwave scatterometer onboard Chinese HY-2 satellite as the outside initial sea surface wind directions, respectively.

3 Results and analysis

The circular or elliptical signature patterns on SAR image shown in Fig. 1 are interpreted as the result of downdraft wind associated with rainfall. In order to make sure that the retrieval sea surface wind speeds from SAR are reliable and analyze the wind structure of the footprint signature patterns of rain cells (i.e., the airflow patterns), we extract sea surface wind speed from SAR image and validate it against NCEP, ASCAT and HY-2 SCAT sea surface wind data, respectively. Then analyze the feature of the wind field of the rain cell patterns on SAR image.

3.1 *Sea surface wind speed retrieval from SAR image*

As mentioned in the above section, sea surface wind speed can be extracted from the NRCS of SAR image by using a suitable GMF and outside wind directions. We use CMOD4 as the GMF in this study. The NRCS of SAR image used in this study can be calibrated by the following formula (Luscombe, 2008):

$$\sigma_0 = |DN|^2/A\,, \tag{2}$$

where σ_0 is the NRCS value, DN is the digital value of SAR data and A is the gain value corresponding to the range sample. The gain value A, incidence angle and the radar azimuth can be read in the Radarsat-2 SAR Look-up Tables (LUTs) files. The azimuth is used to calculate the relative wind direction.

We extract sea surface wind fields from SAR image (shown in Fig. 1) using wind directions of NCEP, ASCAT and HY-2 SACT, respectively. The sea surface wind speed retrieval results are shown in Fig. 2.

As shown in Fig. 2, the SAR wind speed field and compared sea wind are shown at the same time. The color coded arrows represent the outside wind vectors used for SAR wind speed retrieval. That most of the color coded arrows are identical in the SAR wind speed field background means that there are differences between these two wind speeds. Their agreement increases when the color coded arrows disappear in the SAR wind field. In order to get the quality of the retrieval wind speeds, we validate them again NCEP, ASCAT and HY-2 SCAT sea surface wind speeds, respectively. The statistics of validation results used in this study are mean bias (Bias) and root mean square error (RMSE). The mathematic expression of them can be found in Ye et al. (2014, 2015). Additionally, the SAR wind speeds were averaged over an area of diameter of 25 km (for ASCAT and HY-2 SCAT) or 1 degree (for NCEP) so that two measurements would be comparable. The validation results and scatter plot comparisons are shown in Fig. 3.

As listed in Fig. 3, the Bias of validations against NCEP, ASCAT and HY-2 SCAT are –0.21 m/s, –0.69 m/s, and –1.31 m/s, respectively. The RMSEs are 1.48 m/s, 1.64 m/s and 2.14 m/s, respectively. The differences among these validations may be caused by the time separations between SAR and the compared wind speed. The SAR image in this study was acquired on May 24, 2012 at 22:20 UTC. The compared winds were measured at different time of NCEP at 00:00 UTC (May 25, 2012), ASCAT at 01:43 UTC (May 25, 2012) and HY-2 SCAT at 19:21 UTC (May 24,

2012). In other words, the temporal difference between SAR and NCEP is 1 h and 40 min. The values are 3 h and 23 min for ASCAT, 2 h and 59 min for HY-2 SCAT. The closest time between SAR and NCEP may leads to the minimum validation statistics with Bias of –0.21 m/s and RMSE of 1.48 m/s. The largest error validated against HY-2 SCAT with the Bias of –1.31 m/s and the RMSE of 2.14 m/s may also be caused by the microwave frequencies which the SAR and scatterometer operate at. The SAR and ASCAT used in this study are operating at C-band, but HY-2 SCAT is operating at Ku-band. Ku and C-band are not the same sensitive to the effect of rainfall.

These validation results represent the same error level for

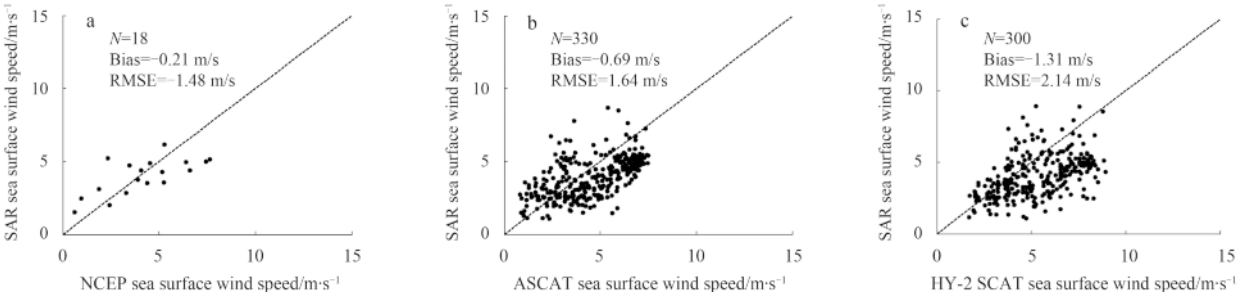

Fig. 3. Scatter plot comparisons of sea surface wind speeds between retrieval from SAR and validated measurements. a. NCEP, b. ASCAT and c. HY-2 SCAT. *N* is the validated data number, Bias the mean bias and RMSE the root mean square error.

other research, e.g., the Bias is 0.45 m/s and RMSE is 2.28 m/s for time separations of less than 1 h, the Bias is –0.63 m/s and RMSE is 2.01 m/s for time separations of less than 15 min in Thompson et al. (2001). The Bias is 0.83 m/s and the RMSE is 1.74 m/s in Xu et al. (2008). Their SAR retrieval wind speeds are both validated with QuikSCAT (an American microwave satterometer satellite). In a word, the wind speeds extracted from SAR image in this study are reliable.

3.2 *The feature of wind in footprint signature pattern and analysis*

We analyze the feature of the footprint patterns of rain cells shown in Fig. 1. The eight patterns (with the Numbers of A–H) are all the same feature as typical signature pattern associated with rain cell. I.e., the pattern is a circular or elliptical pattern with brighter than the surrounding on one side and darker on the opposite side. Figure 4 shows the NRCS of rain cell Pattern A, taken from the circular curve with a diameter of 0.17 *D*, 0.25 *D* and 0.33 *D*, respectively. *D* is the diameter of the outer circular edge of the rain cell footprint pattern.

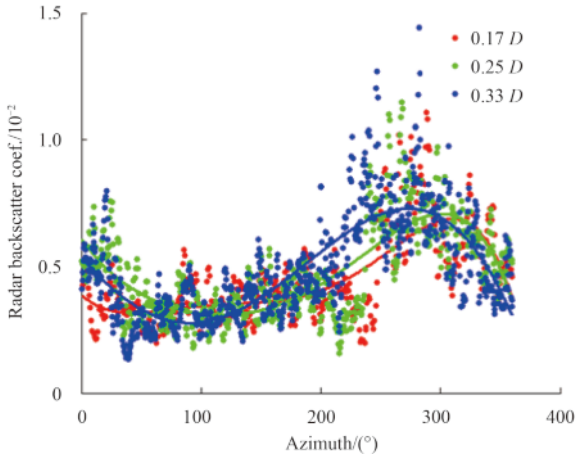

Fig. 4. NRCS of rain cell footprint Pattern A, taken from the circular curve with a diameter of 0.17 *D*, 0.25 *D* and 0.33 *D*, respectively. *D* is the diameter of the outer circular edge of rain cell footprint pattern. Solid lines in the figure are the polynomial fitting curve.

As shown in Fig. 4, the NRCS taken from the circular curve with different diameters have the same variational trend and they can be fitted as polynomial function. The azimuth with maximal NRCS is the same as the direction of background wind field. By using these features, we can get the direction of the ambient wind.

Figure 5 shows the curve of NRCS taken from the transect profile which goes through both minimal and maximal NRCS points. The origin of the horizontal axis locates the endpoint in the side with maximal NRCS. As shown in Fig. 5, we can also find out that the NCRS values on the left side are larger but smaller on the opposite side.

These dimensional characters mentioned above are caused by airflow associated with rain cells. Precipitation from a rain cell can produces downdraft (downward airflow). When this downdraft reaches sea surface, it spreads radially outward as local surface wind. In the case of a strong ambient wind field, the downwind side of the rain cell is imaged brighter and the upwind side darker than the surrounding area. The pattern is usu-

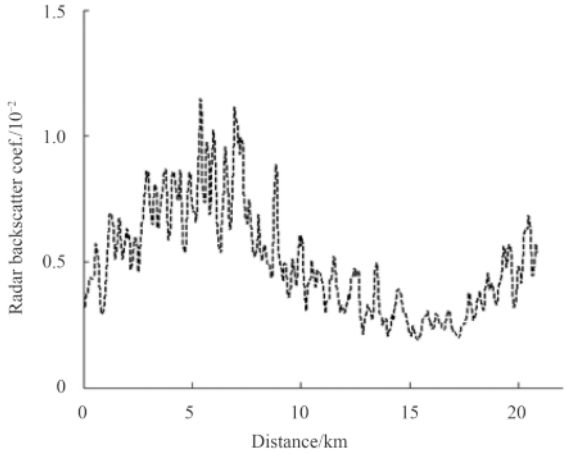

Fig. 5. Curve of NRCS taken from the transect profile which goes through both minimal and maximal NRCS area shown in Fig. 4. The origin of the horizontal axis locates the endpoint on the side with maximal NRCS.

ally less bright in the center, where the downdraft reaches sea surface vertically with the horizontal wind speed is lowest. The brightness increases downwind as the horizontal wind vectors of radially-spreading downdraft add positively to the ambient wind vectors, the brightness decreases upwind as the two vectors add negatively (Alpers and Melsheimer, 2004). The footprint signature pattern caused by downdraft associated with rain cell is shown schematically in Fig. 6.

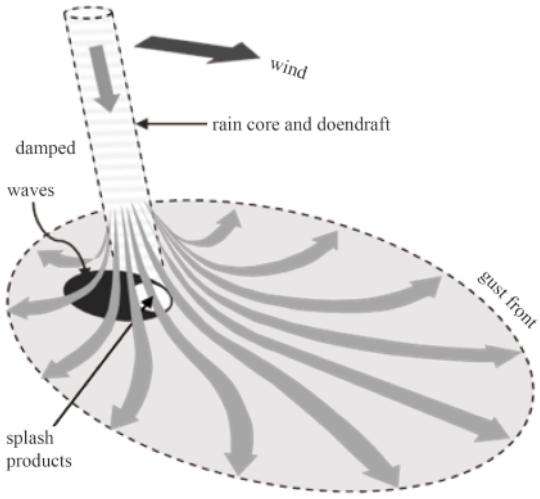

Fig. 6. Schematic sketch of the downdraft associated with rain cell (redraw after Alpers and Melsheimer (2004) and Atlas (1994)).

We extract the sea surface wind speeds of the eight footprint patterns with No. A–H by using CMOD4 GMF again. We use the wind direction features on image pattern itself shown in Fig. 4 instead of outside wind sources, i. e., the azimuth with maximal NRCS is the direction of wind field. Figure 7 shows the wind speed image derived from the sub-image of pattern A shown in Fig. 1. We can also see the circular footprint in the figure with a typical signature pattern associated with rain cell.

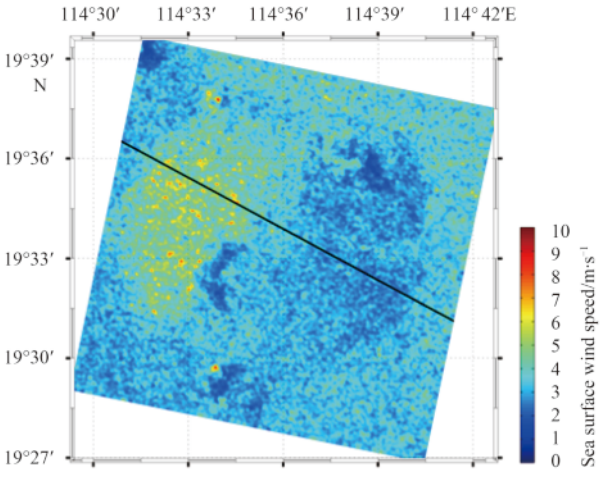

Fig. 7. Wind speed image derived from the sub-image of pattern A shown in Fig. 1. The black line is the transect which superposes to the wind ambient vectors and goes through the center of the circular footprint of rain cell.

We plot the curve of wind speeds taken from the transect profile shown in Fig. 7, the cure is shown in Fig. 8. The transect shown in Fig. 7 superposes to the wind ambient vectors and goes through the center of the circular footprint. Thus, the wind speeds in this transect are linear added by the speeds of downdraft caused by rain cell and the ambient wind speeds.

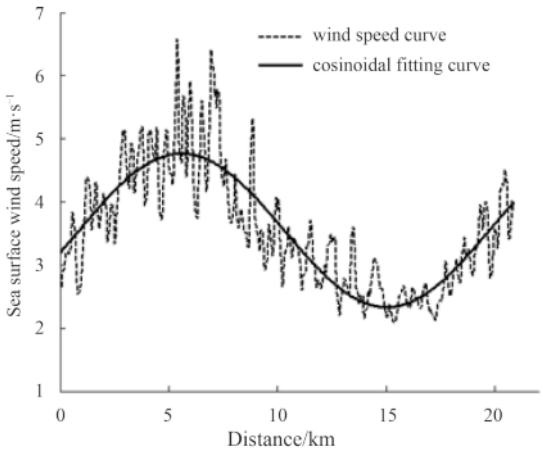

Fig. 8. Curve of wind speed taken from the transect profile shown in Fig. 7. The black solid line is the fitting cosine curve. The origin of the horizontal axis is the location of the leftmost point in the black line shown in Fig. 7.

We try fitting the wind speed curve shown in Fig. 8 as a cosinodal function. The form for the cosine expression is

$$V = V_{\mathrm{m}} \cos\left[1/(2\pi) Dx + x_0\right] + V_0, \tag{3}$$

where V is the wind speed retrieval from SAR image, D is the diameter of the circular signature pattern of rain cell, V_0 is the wind speed of background. The absolute value of V_{m} is the maximal horizontal wind speed caused by downdraft associated with rain cell, x_0 is the initial phase that depends on the location of the origin, x is the distance. V_{m}, D, x_0 and V_0 can be obtained by least squares fitting. These coefficients for Patterns A–H shown in Fig. 1 are listed in Table 1. The parameter R in the table is the linear correlation coefficient of the cosinoidal function fitting.

As listed in Table 1, the background wind speeds (the values of V_0 listed in Table 1) vary from 2.5 m/s to 4.5 m/s, which are not significant different from the wind speeds shown in Fig. 2. That is

Table 1. Coefficients of fitting as cosinodal function for the wind speeds taken from the transect profile which superposes to ambient wind vectors and goes through to the center of circular footprint signature pattern shown in Fig. 1

Pattern No.	Parameter				
	V_{m}	D	x_0	V_0	R
A	–1.22	18.9	1.18	3.5	0.86
B	1.15	12.0	–1.29	2.8	0.83
C	0.82	8.7	–2.06	2.5	0.80
D	1.13	11.5	–1.16	3.1	0.86
E	1.85	10.1	–1.18	3.8	0.82
F	1.54	5.8	–1.69	3.5	0.89
G	2.34	10.3	–1.81	3.9	0.84
H	2.80	16.5	–1.55	4.5	0.83

to say, the background wind speeds extracted by the fitting method mentioned in Fig. 8 and Eq. (3) approximate the wind speeds retrieval from SAR image by outside wind directions. The diameters of circular signature patterns of rain cells (the values of D listed in Table 1) have the values of kilometers or tens of kilometers. The largest signature circle is Pattern A with a diameter of 18.9 km, the smallest is pattern F with a diameter of 5.8 km. The horizontal wind speeds (V_{m}) caused by rain cells are all much smaller than the background wind speed (V_0). For this reason, the typical signature with brighter on one side and darker on the opposite side appears. A circular signature pattern which is brighter than surrounding area would appear when V_{m} is much larger than V_0.

The wind speeds taken from the transect profile which superposes to the wind ambient vectors and goes through the center of the circular footprint of rain cell can be fitted as a cosinodal function. Take Pattern A shown in Fig. 7 as an example, Fig. 8 shows the wind speed curve and the fitting curve. The eight linear correlation coefficients of fitting are no less than 0.80 (Table 1). These wind speeds feature is caused by the downdraft associated with rainfall.

4 Conclusions

In this study, we extract the sea surface wind speeds from RADARSAT-2 SAR image in high resolution by using GMF of CMOD4 with the outside wind directions of NCEP, ASCAT and HY-2 SCAT, respectively. We also validate the retrieval wind speeds and the validation results show they have the same error level with other studies.

The circular footprint signature patterns with brighter on one side and darker on the opposite side on SAR image can be interpreted as the sea surface wind speed (or sea surface roughness) variety caused by downdraft associated with rain cell. The data analysis results show that NRCS taken from the circle curve with different diameters have the same variational trend and the azimuth with maximal NRCS is the direction of background wind.

The wind speeds taken from the transect profile which superposes to the wind ambient vectors and goes through the center of the circular footprint of rain cell can be fitted as a cosine or sine curve in high linear correlation. By using this fitting and analysis method, the wind speeds and the size of circular footprint signature pattern caused by rain cell can be acquired.

Acknowledgments

The MetOp-A/ASCAT data are downloaded from PO.DAAC/JPL, NASA (https://podaac.jpl.nasa.gov/). The NCEP final operational global analysis data are downloaded from NCEP (http://rda.ucar.edu/). The authors thank these organizations offering the data.

References

Alpers W, Cheng C M, Shao Yun, et al. 2007. Study of rain events over the South China Sea by synergistic use of multi-sensor satellite and ground-based meteorological data. Photogrammetric Engineering & Remote Sensing, 73(3): 267–278

Alpers W, Melsheimer C. 2004. Chapter 17: rainfall. In: Jackson C R, Apel J R, eds. Synthetic Aperture Radar Marine User's Manual. Washington, DC: National Oceanic and Atmospheric Administration, 355–371

Atlas D. 1994. Origin of storm footprints on the sea seen by synthetic aperture radar. Science, 266(5189): 1364–1366

Chan P W, Cheng C M, Aplers W. 2010. Study of wind fields associated with subtropical squall lines using Envisat Synthetic Aperture Radar images and ground-based weather radar data. International Journal of Remote Sensing, 31(17–18): 4897–4914

Contreras R F, Plant W J. 2006. Surface effect of rain on microwave backscatter from the ocean: measurements and modeling. Journal of Geophysical Research: Atmospheres, 111(C8): doi: 10.1029/2005JC003356

Friedman K S, Li Xiaofeng. 2000. Monitoring hurricanes over the ocean with wide swath SAR. Johns Hopkins APL Technical Digest, 21(1): 80–85

Gan Xilin, Huang Weigen, Yang Jingsong, et al. 2007. The study of fine structure of a mesoscale thunderstorm from SAR image. Remote Sensing Technology and Application (in Chinese), 22(2): 246–250

Hersbach H, Stoffelen A, de Haan S. 2007. An improved C-band scatterometer ocean geophysical model function: CMOD5. Journal of Geophysical Research, 112(C3): doi: 10.1029/2006JC003743

Houze Jr R A. 1997. Stratiform precipitation in regions of convection: A meteorological paradox?. Bulletin of the American Meteorological Society, 78(10): 2179–2196

Jiang Xingwei, Lin Mingsen, Liu Jianqiang, et al. 2012. The HY-2 satellite and its preliminary assessment. International Journal of Digital Earth, 5(3): 266–281

Lin Hui, Xu Qing, Zheng Quanan. 2008. An overview on SAR measurements of sea surface wind. Progress in Natural Science, 18(8): 913–919

Lin I I, Alpers W, Khoo V, et al. 2001. An ERS-1 synthetic aperture radar image of a tropical squall line squall compared with weather radar data. IEEE Transactions on Geoscience and Remote Sensing, 39(5): 937–945

Luscombe A. 2008. RADARSAT-2 Product Format Definition. Richmond, Canada: MacDonald, Dettwiler and Associates Ltd

Melsheimer C, Alpers W, Gade M, et al. 2001. Simultaneous observations of rain cells over the ocean by the synthetic aperture radar aboard the ERS satellites and by surface-based weather radars. Journal of Geophysical Research: Atmospheres, 106(C3): 4665–4677

Morena L C, James K V, Beck J. 2004. An Introduction to the RADARSAT-2 mission. Canadian Journal of Remote Sensing, 30(3): 221–234

Quilfen Y, Chapron B, Elfouhaily T, et al. 1998. Observation of tropical cyclones by high-resolution scatterometry. Journal of Geophysical Research, 103(C4): 7767–7786

Stofflen A, Anderson D. 1997. Scatterometer data interpretation: Estimation and validation of the transfer function CMOD4. Journal of Geophysical Research, 102(C3): 5767–5780

Thompson D R, Monaldo F M, Beal R C, et al. 2001. Combined estimates improve high-resolution coastal wind mapping. EOS, 82(41): 469–484

Xu Feng, Li Xiaofeng, Wang Peng, et al. 2015. A backscattering model of rainfall over rough sea surface for Synthetic Aperture Radar. IEEE Transactions on Geoscience and Remote Sensing, 53(6): 3042–3054

Xu Qing, Lin Hui, Zheng Quanan, et al. 2008. Evaluation of ENVISAT ASAR data for sea surface wind retrieval in Hong Kong coastal waters of China. Acta Oceanologica Sinica, 27(4): 57–62

Yang Jingsong, Huang Weigen, Zhou Changbao, et al. 2001. Coastal ocean surface wind retrieval from SAR imagery. Journal of Remote Sensing (in Chinese), 5(1): 13–16

Ye Xiaomin, Lin Mingsen, Song Qingjun. 2014. Research on validation methods of satellite radar altimeter retrieved sea surface wind speed and significant wave height using in-situ data. Remote Sensing Technology and Application (in Chinese), 29(1): 26–32

Ye Xiaomin, Lin Mingsen, Xu Ying. 2015. Validation of Chinese HY-2 satellite radar altimeter significant wave height. Acta Oceanologica Sinica, 34(5): 60–67

Zhang Yi, Jiang Xingwei, Song Qingtao, et al. 2014. Coastal wind field retrieval from polarimetric synthetic aperture radar. Acta Oceanologica Sinica, 33(5): 54–61